Published in Journal of Metamorphic Geology 12, 667-680, 1994
which should be used for any reference to this work

Rb–Sr and U–Pb isotope studies on migmatites from the Schwarzwald (Germany): constraints on isotopic resetting during Variscan high-temperature metamorphism

A. KALT,[1] B. GRAUERT[2] AND A. BAUMANN[2]
[1]*Minerlogisch-Petrographisches Institut, Im Neuenheimer Feld 236, D-69120 Heidelberg, Germany*
[2]*Zentrallabor für Geochronologie, Corrensstr. 24, D-48149 Münster, Germany*

ABSTRACT Mineral and isotope studies were undertaken on migmatites from the Schwarzwald, Moldanubian zone of the Variscan belt. The aims of the study were to date the migmatite formation and to determine the processes involved in migmatization in order to evaluate their influence on isotopic resetting. Textural evidence and the comparison of mineral compositions from leucosomes and mesosomes of two centimetre-scale migmatite profiles, respectively, suggest that migmatitic textures and mineral assemblages were formed by metamorphic segregation (deformation-enhanced mass transport) rather than by partial melting (anatexis). The results of Rb–Sr thin-slab dating on these profiles indicate that Sr isotopes were not completely reset during migmatization. No true isochron ages, but ages of approximate isotopic homogenization were obtained on the thin slabs by calculating $^{87}Sr/^{86}Sr$ ratios back to various stages in their evolution. The coincidence of these Rb–Sr data with U–Pb ages of monazites from migmatites and non-migmatitic gneisses shows that gneisses and migmatites were formed during the same high-temperature event in the Carboniferous (330–335 Ma). The observation that high-temperature metamorphism failed to equilibrate Sr isotopes on the centimetre-scale imposes limitations on the use of conventional whole-rock isochron techniques in dating migmatites.

Key words: Rb–Sr thin-slab dating; Schwarzwald; U–Pb monazite dating; Variscan migmatites.

INTRODUCTION

Migmatites are characteristic rocks of high-grade metamorphic complexes. They are especially widespread within the Moldanubian zone of the Variscan belt in Europe. Although subject to numerous studies, the evolution of migmatitic rocks in general as well as of Variscan migmatites in particular is still not very well constrained and is a matter of discussion.

Recent papers on migmatites have above all been concerned with the problem of generating granitic melts from metasedimentary rocks and have therefore focused mainly on experimental topics. The results of melting experiments clearly indicate that migmatites may be derived from various metamorphic rocks by partial melting at equilibrium conditions (Tuttle & Bowen, 1958; Johannes & Gupta, 1982; Thompson, 1982; Clemens & Vielzeuf, 1987; Le Breton & Thompson, 1988; Rutter & Wyllie, 1988), and at non-equilibrium conditions (Rubie & Brearley, 1990). Melting temperature and the amount of melt generated are strongly dependent on water activity (Conrad *et al.*, 1988; Johannes & Holtz, 1990; Holtz & Johannes, 1991) and the composition of the starting material (Patiño Douce & Johnston, 1991; Skjerlie *et al.*, 1993).

Studies on natural migmatites (Sawyer & Robin, 1986) as well as theoretical considerations (Lindh & Wahlgren, 1985) suggest that stromatic migmatites (in the sense of Johannes & Gupta, 1982) at least may form by metamorphic segregation at subsolidus conditions. Attempts to distinguish between melt-present and melt-absent migmatite formation on the basis of textures and chemical composition have been made (McLellan, 1983, Sawyer & Barnes, 1988, Mazurek, 1992) but are generally hampered by the lack of applicable criteria. While textural relations may at least in some cases give evidence of partial melting (McLellan, 1983; Vernon & Collins, 1988), comparison of chemical compositions of natural leucosomes and mesosomes with compositions derived from melting experiments constrains only the *conditions* of migmatite formation, provided the *process* of partial melting has been independently ascertained for the studied rock.

Knowledge of the processes involved in migmatite formation and information on the scale and extent of chemical equilibrium attained are essential requirements for the interpretation of geochronological data on these rocks, as resetting of isotope systems is strongly dependent on the physical and chemical parameters of metamorphism such as temperature, pressure, deformational regime, absence or presence of fluids and melts. These implications

are often not considered when dating migmatites. Especially for the Variscan belt, U–Pb ages of accessory phases like zircon (Steiger *et al.*, 1973; Barbey *et al.*, 1989) as well as Rb–Sr ages calculated from best fit lines for large whole rock samples (Hofmann & Köhler, 1973) or isolated mesosome and leucosome domains (Grauert *et al.*, 1974) have commonly been interpreted as the age of migmatite formation. In these studies, complete isotopic resetting over large distances during migmatite formation is simply assumed without considering the specific conditions of migmatite formation.

The purpose of this paper on migmatites from the Schwarzwald is thus twofold. The first intention is to evaluate the role of partial melting for these rocks on the basis of mineral and textural data. The second aim is to date migmatite formation in the Schwarzwald and to constrain the degree of isotope resetting at the time of migmatite formation by using the Rb–Sr thin-slab dating method.

GEOLOGICAL SETTING AND PREVIOUS GEOCHRONOLOGICAL WORK

The Schwarzwald in south-western Germany forms part of the internal zone of the Variscan belt (Fig. 1). Its largest basement unit is the Central Schwarzwald Gneiss Complex (CSGC, Krohe & Eisbacher, 1988). It is dominated by high-grade metamorphic rocks and granites and was tectonically emplaced over low-grade metamorphic rocks of the Saxothuringian zone to the north and over volcanic and sedimentary sequences to the south during Variscan convergence (Eisbacher *et al.*, 1989). A second high-grade basement unit, the Southern Schwarzwald (Fig. 1) borders further to the south.

The metamorphic units of the CSGC and of the Southern Schwarzwald are dominated by metapsammitic to metapelitic gneisses. Within the CSGC, more variegated lithologies and minor occurrences of granulites and retrogressed high-pressure rocks are locally intercalated in the gneisses. In both units the pervasive metamorphic overprint of the gneisses is of the low-pressure high-temperature type and is concurrent with the development of the dominant foliation (D3, Flöttmann & Kleinschmidt, 1989) in these rocks. The gneisses were partially transformed to migmatites, whereby gneissose textures were overprinted by a synmigmatitic deformation (D4, Flöttmann & Kleinschmidt, 1989).

Several geochronological studies have been carried out on the basement rocks of the Schwarzwald. The intrusion of granitic rocks in the Schwarzwald is fairly well dated at 340–310 Ma (Brewer & Lippolt, 1974; Wendt *et al.*, 1974; Todt, 1976; Von Drach, 1978), granites older than 325 Ma having been intruded within a compressional regime during the tectonic emplacement of the CSGC, and younger intrusions being related to subsequent crustal extension (Echtler & Chauvet, 1991/92).

The *P–T–t* evolution of gneisses and migmatites in the Schwarzwald, however, is rather poorly constrained and the obtained results are ambiguous. U–Pb analyses of

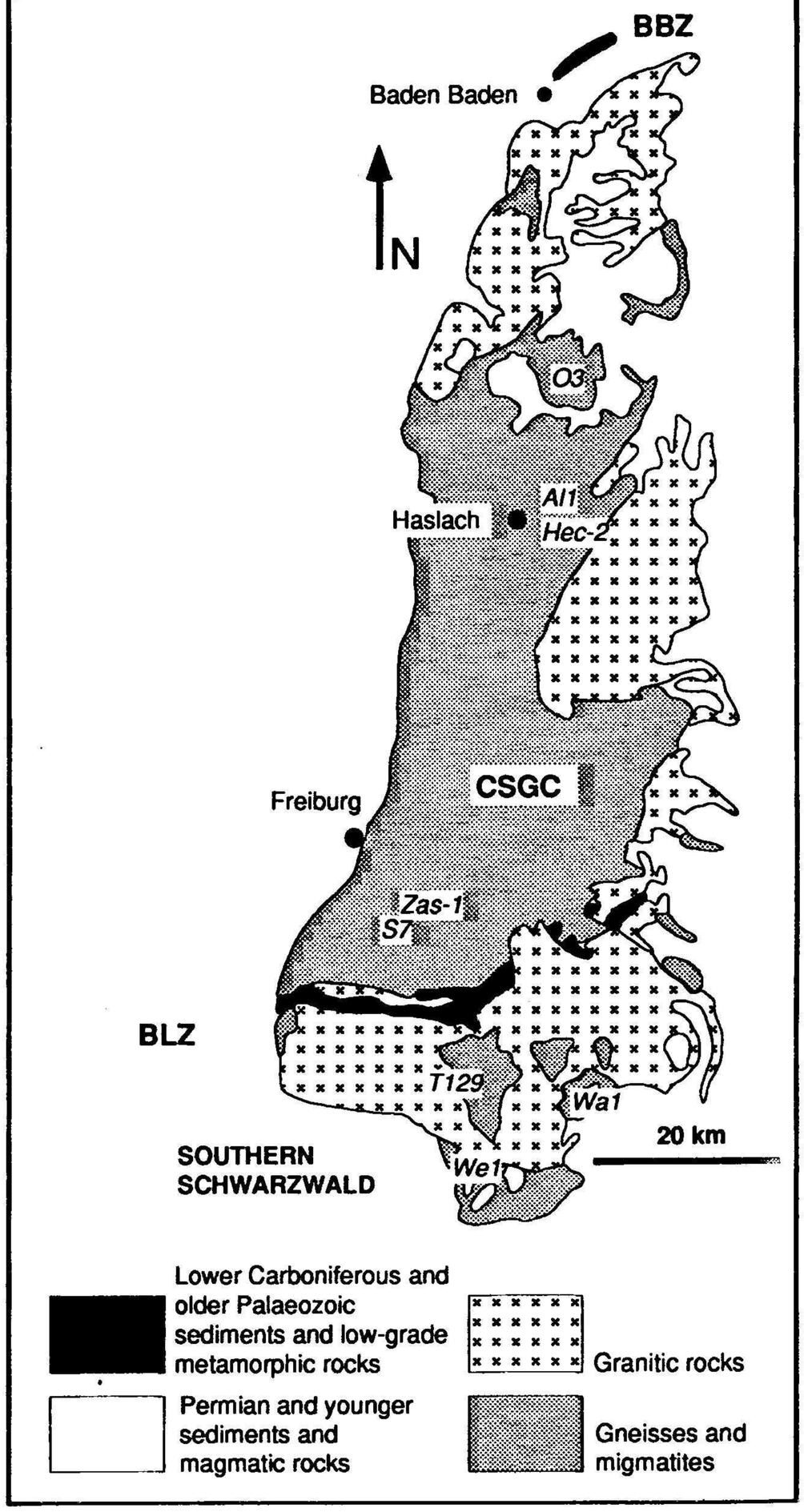

Fig. 1. Simplified geological sketch map of the Schwarzwald (modified after Wickert & Eisbacher, 1988; Wimmenauer & Stenger, 1989), showing the main basement units and the sample sites (marked in italics). Samples O3, Al1, Zas–1, S7, T129, Wa1, and We1 were taken for U–Pb dating on monazites. Samples Hec-2 and Zas-1 were taken for Rb–Sr thin slab dating. Abbreviations: BBZ, Baden-Baden-Zone; BLZ, Badenweiler-Lenzkirch-Zone; CSGC, Central Schwarzwald Gneiss Complex. Inset: the Schwarzwald within the Variscan setting. Abbreviations: RHZ, Rhenohercynian Zone; STZ, Saxothuringian Zone; MZ, Moldanubian Zone.

zircons from gneisses point to magmatic and/or metamorphic events between 520 and 480 Ma (Todt & Büsch, 1981; Kober, 1986; Kober, 1987). Ordovician U–Pb intercept ages of zircon fractions from migmatites (Steiger *et al.*, 1973) and Rb–Sr ages calculated from best fit lines for migmatite whole rock samples (Hofmann & Köhler, 1973) were interpreted as the age of migmatite formation. Petrological constraints on these Early Palaeozoic ages are lacking.

On the other hand, Ar–Ar and Rb–Sr mineral ages from metamorphic rocks range between about 375 and 325 Ma (Von Drach, 1978; Hradetzky, 1989), thus clearly indicating a Late Variscan tectonothermal event. Further, high-pressure metamorphism of eclogites has recently been dated at 334–337 Ma by Sm–Nd isochrons on garnet, clinopyroxene and whole rock samples from eclogites (Kalt *et al.*, 1994), giving a maximum age for high-temperature metamorphism and migmatization as most eclogites shared their retrograde low-pressure high-temperature stage with the adjacent gneisses and migmatites.

PETROGRAPHY AND MINERAL CHEMISTRY

Samples

The samples for this study were taken in order to (1) date low-pressure high-temperature metamorphism and migmatite formation in the Schwarzwald and (2) test the degree of Rb–Sr isotope equilibration achieved during migmatization (for sample sites see Fig. 1). For the first purpose, four migmatite samples and four gneiss samples were chosen for U–Pb monazite dating. As the samples differ in terms of textures, mode, degree of migmatization and provenance, it is possible to check whether the age of the last thermal overprint is the same throughout the Schwarzwald and whether low-pressure high-temperature metamorphism and migmatization occurred during two distinct geological events as suggested by previous work. For the second purpose, two migmatite samples were chosen for Rb–Sr thin-slab dating. The samples are of psammitic composition and thus representative of the majority of migmatites from the Schwarzwald.

Textures and mineral assemblages

Samples taken for U–Pb analyses on monazites are not described in detail here; their mineral assemblages are listed in Table 2.

The two samples taken for Rb–Sr thin-slab dating (Hec-2 and Zas-1) are quite similar in terms of mineral assemblages but differ in their macroscopic textures. Both migmatite samples show compositional banding on millimetre to centimetre scale (Figs 5a & 6a) which is defined by alternations of coarse-grained leucosomes and medium- to fine-grained mesosomes (both in the sense of Ashworth, 1985). Melanosomes are only rarely observed as small flakes or selvedges of biotite adjacent to leucosomes. In sample Hec-2 compositional banding is very pronounced. Mesosomes have a marked internal foliation, represented by orientated biotites, which is concordant with compositional banding. Leucosomes show isotropic textures. Most of them are parallel or subparallel to banding but a few leucosomes also form pods which partly displace and break up banding and mesosome foliation. Sample Zas-1 shows essentially the same features, but the portion of non-concordant leucosomes is higher so that compositional banding is in places replaced by a more complex geometry.

The main minerals in mesosomes of both samples are biotite, plagioclase, and quartz. Minor phases are alkali feldspar, sillimanite, as well as rounded or sickle-shaped garnet relics (and muscovite relics in sample Hec-2) in large plagioclase grains. Biotites have fuzzy, irregularly shaped rims, sometimes altered to chlorite and often framed by ilmenite. Plagioclase is anhedral to subhedral and commonly twinned. It has inclusions of drop-shaped quartz as well as K-feldspar and may be altered to sericite. Some plagioclase grains display weak zoning and/or patchy extinction, both pointing to compositional variations or domain misorientation. Quartz grains are anhedral and show serrated grain boundaries, subgrains, and undulatory extinction.

Alkali feldspar forms small anhedral grains. Sillimanite forms rare swarms of tiny needles within plagioclase, or at biotite margins. Accessory phases are apatite, monazite, and zircon commonly observed in and around biotite, as well as secondary chlorite and muscovite formed from biotite.

Leucosomes consist of plagioclase, quartz, some alkali feldspar, and minor biotite. The main mineral is plagioclase which forms large euhedral to subhedral grains showing the same internal features as in the mesosomes. Quartz grains are anhedral to subhedral and show serrated grain boundaries, subgrains, and undulatory extinction. Alkali feldspar is much more abundant than in the mesosomes, the large perthitic grains including all other minerals. Rare myrmekitic intergrowths can be observed between plagioclase and alkali feldspar grains. Biotite forms small flakes in alkali feldspar or at grain boundaries. Accessory phases are only present as inclusions in biotite grains.

Mineral chemistry

Analytical techniques are described in the Appendix. Analytical data on biotite and plagioclase are available from the authors on request.

Plagioclase. In order to explore the role of partial melting processes, concentration profiles for Na, Ca and K were determined for several plagioclase grains. If melting had been a significant process for migmatite formation, plagioclase grains in leucosomes and in mesosomes should have different compositions, respectively (Johannes, 1985). According to the experimental results of Tsuchiyama & Takahashi (1983), Johannes (1989) and Holtz & Johannes (1991), melting of plagioclase in various natural and model

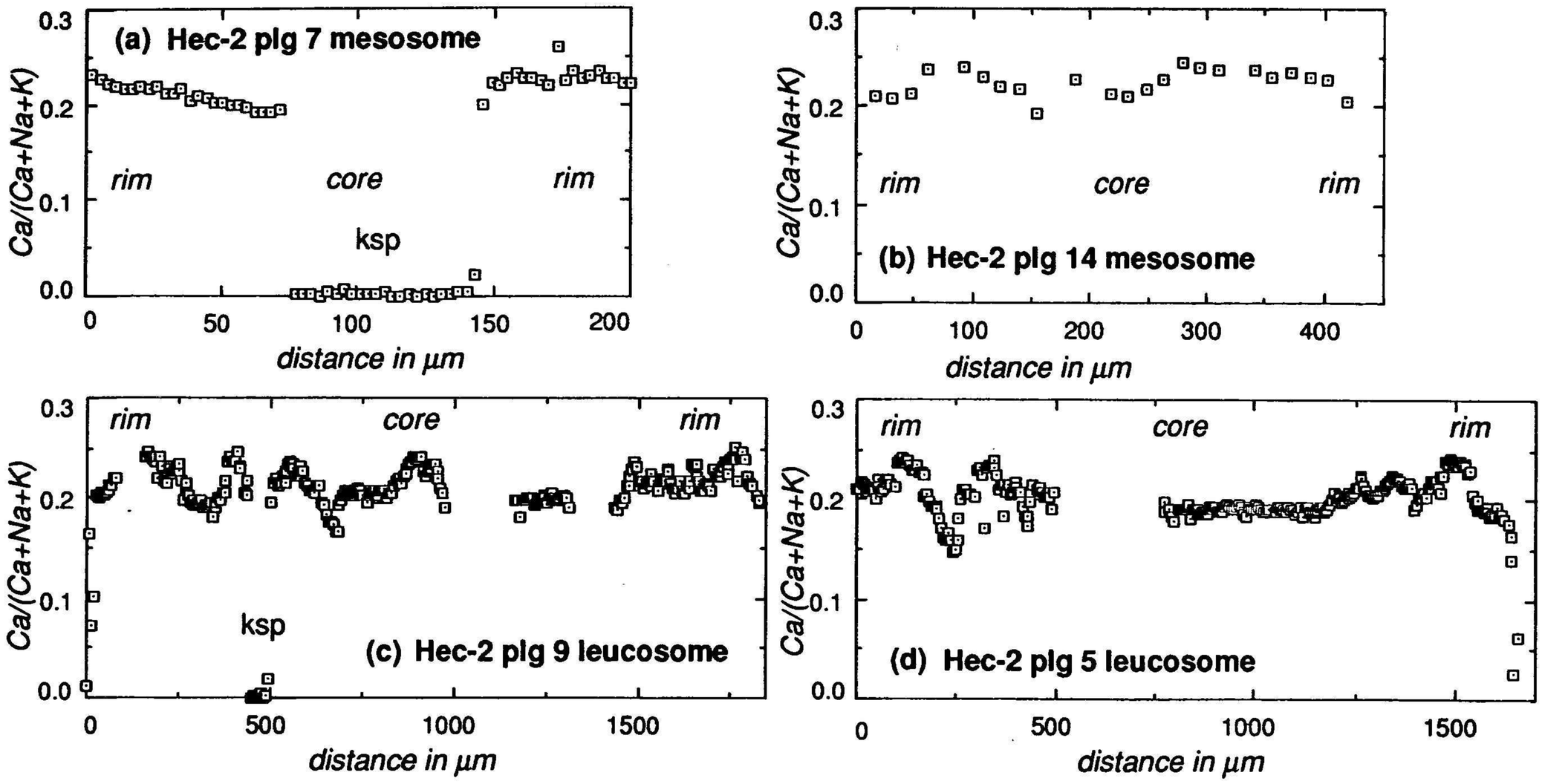

Fig. 2. Representative zoning patterns showing the variation of An contents in plagioclase grains from mesosomes and leucosomes of sample Hec-2. For explanation see text.

systems leads to Ab-rich melts and An-rich residual plagioclase grains.

Figures 2 & 3 show representative zoning patterns of plagioclase grains from samples Hec-2 and Zas-1. Systematic differences between zoning patterns of mesosome and leucosome plagioclase grains cannot be recognized. The An contents in cores of individual mesosome and leucosome grains vary only on a small scale and rather irregularly so that most plagioclase grains tend to have fairly flat An core patterns (Figs 2a, b & 3a–d) while others display weak, oscillatory zoning patterns (Fig. 2c,d). The very low values for An in the cores of some

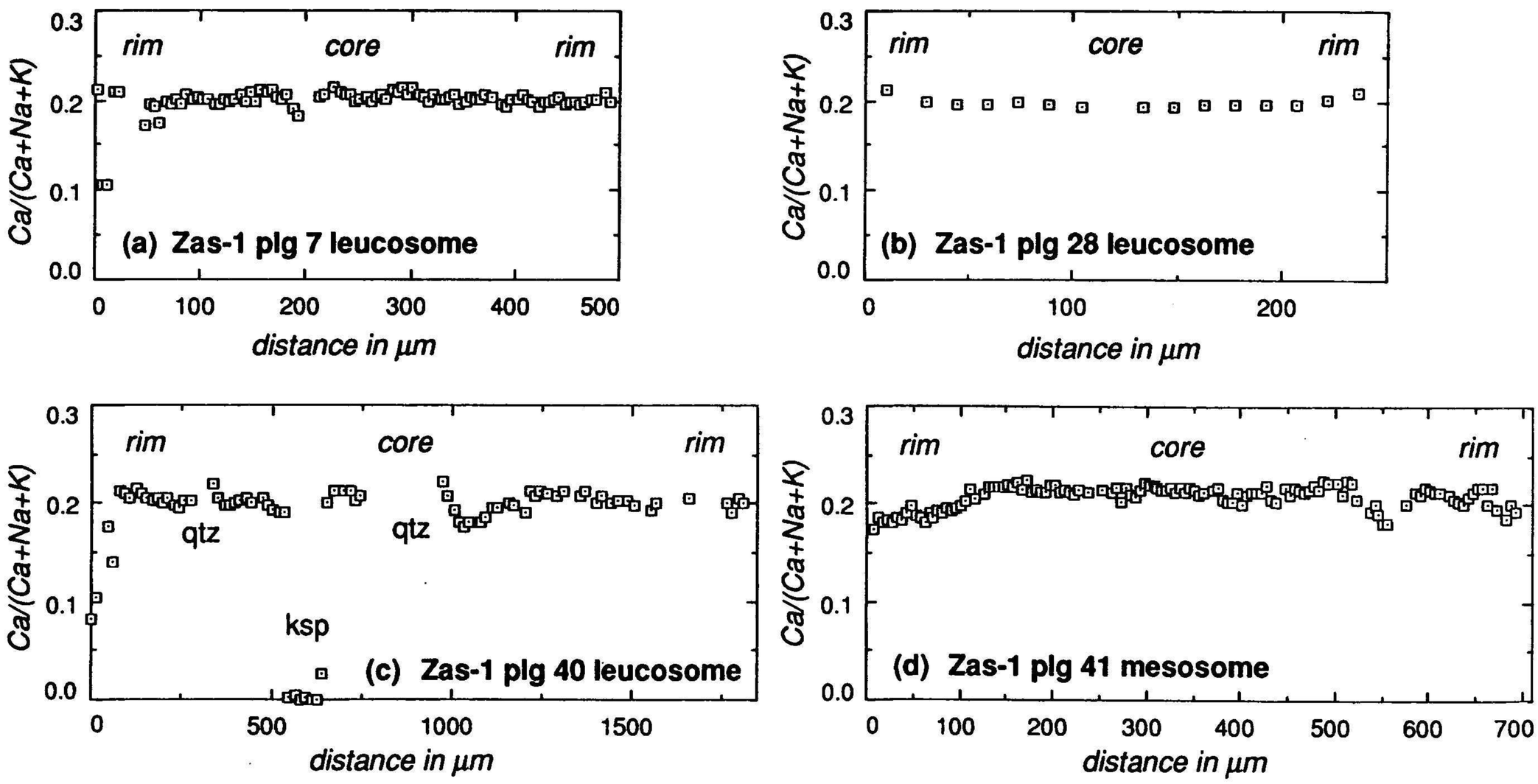

Fig. 3. Representative zoning patterns showing the variation of An contents in plagioclase grains from mesosomes and leucosomes of sample Zas-1. For explanation see text.

grains (Figs 2a & 3c) correspond to K-feldspar inclusions. Plagioclase rims display different features. At most rims a slight decrease in An content can be observed (Fig. 2b, c right margin, d left margin, 3d). In some leucosome grains, the outermost rims show a steep decrease in An contents, in all cases due to increase in Ab contents and not in Or contents (Figs 2c, d & 3c). A few grains also show slight An enrichment at their rims (Figs 2b & 3a).

Consequently, the diverse An patterns of plagioclase grains from the two samples do not support a model of leucosome formation by partial melting as proposed for example by Johannes & Gupta (1982). The only feature consistent with partial melting is the An depletion at the rims of some grains. These narrow An-depleted rims may have crystallized from a melt as suggested by experimental results (see above). The An-enriched parts at the inner sides of the An-depleted outermost rims (Fig. 2c, d) may correspond to diffusively Ab-depleted parts that remained solid during partial melting. As these observations can only be made in a few grains it must be concluded that – if partial melting took place at all – the amount of melt must have been insignificant.

The observed An patterns are more consistent with those obtained from studies on mass transport mechanisms in rocks deforming at high temperatures (McCaig & Knipe, 1990; Yund & Tullis, 1991). The relevant transport mechanisms suggested by quartz subgrains and by domain misorientation in plagioclase grains in the studied rocks are diffusive mass transfer along grain boundaries (Coble creep) and within crystal boundaries (Nabarro–Herring creep) as well as dislocation creep (Knipe, 1989). Deformation experiments conducted at high-temperature conditions (Yund & Tullis, 1991) revealed that plagioclase grains recrystallized from an original mixture of two plagioclases (An_1 and An_{79}) were either compositionally equal to the original grains, had an intermediate composition or showed irregular zoning, depending on their position relative to the original grains. Different zoning patterns in the range between An_{20} and An_{37} were also observed in plagioclase grains recrystallized in high-temperature mylonites from Newfoundland (McCaig & Knipe, 1990).

Biotite. If temperatures prevailing during migmatization of the studied rocks had been high enough for dehydration melting of biotite, the compositions of biotites in leucosomes and mesosomes should be significantly different. According to the experimental results of Le Breton & Thompson (1988), Puziewicz & Johannes (1990) and Patiño Douce & Johnston (1991), biotite involved in partial melting reactions should become progressively enriched in Mg and Ti, while Fe should be concentrated in the melt fraction and thus in biotite crystallizing from the melt. Microtextures give no evidence of dehydration melting of biotite as the typical symplectite-like intergrowths of biotite, quartz, potassium feldspar and cordierite (or garnet or ilmenite) formed by this process are absent.

The compositions of mesosome and leucosome biotites of both samples, respectively, are very similar. The compositional variation within individual grains corresponds to the variation range among distinct grains of the two samples. This holds true especially for Mg values, Ti contents as well as for Al^{IV}/Al^{VI} ratios (Table 1). Thus, biotite compositions do not indicate a partial melting event.

Metamorphic evolution

Textures and mineral assemblages of both migmatite samples record at least two different metamorphic stages and conditions. Rare inclusions of almandine–spessartine-rich garnet (and muscovite in sample Hec-2) in mesosome plagioclases of both samples are relics of an early metamorphic mineral assemblage (stage 1). During a later stage, the dominant foliation was formed and the assemblage qtz + pl + kfs + bt + sil became stable (stage 2). The temperature during stage 2 of metamorphism, at least in sample Hec-2, was therefore above that required for the reaction ms + qtz = kfs + als + v which is 575–660° C (a_{H_2O} between 0.5 and 1, Kerrick, 1972) at pressures between 0.23 and 0.6 GPa as indicated by the presence of sillimanite.

The rocks were then migmatized (stage 3) while still within the stability field of the assemblage qtz + pl + kfs + bt + sil. At stage 3, separation of fine-grained biotite-enriched parts (mesosomes) and coarse-grained plagioclase and quartz-rich parts (leucosomes) took place, accompanied by partial break-up of compositional banding and of the stage 2 foliation. Most of this small-scale chemical differentiation was probably achieved by deformation-enhanced and most likely also by fluid-enhanced mass transport as opposed to partial melting and mineral reactions. Evidence for this is (1) the absence of discordant leucosome veins, (2) the fact that all leucosomes are parallel or subparallel to foliation and banding, suggesting that leucosome formation was accompanied by deformation, (3) the absence of unequivocal evidence for partial melting under equilibrium conditions from plagioclase and biotite compositions, (4) the absence of microstructural evidence for partial melting (e.g. Vernon & Collins, 1988), (5) subgrain formation in quartz grains and slightly different lattice orientation within plagioclase grains, consistent with diffusive mass transport and dislocation creep, respectively, (Knipe, 1989), and (6) the lack of reaction textures in conjunction with identical mineral parageneses at stages 2 and 3.

The fact that most minerals obviously remained solid during migmatite formation (stage 3) and that – if at all – only insignificant amounts of melt were involved, suggests that the solidus temperature was the maximum temperature reached by these rocks. As there are no constraints on water activity at the time of migmatite formation, the solidus temperature can only be bracketed by comparison with melting temperatures of comparable vapour-present and vapour-absent model or natural systems.

Table 1. Representative chemical compositions of biotites.

	Zas–1					Hec–2				
	meso grain 1	meso grain 1	leuco grain 2	leuco grain 2	meso grain 3	meso grain 1	meso grain 1	leuco grain 2	leuco grain 2	meso grain 3
SiO_2	35.63	34.48	34.67	34.85	34.86	34.45	34.03	34.73	34.41	34.86
Al_2O_3	19.10	18.48	18.91	18.76	18.56	19.28	18.88	19.11	19.10	19.19
TiO_2	4.01	3.89	3.91	3.56	5.24	2.88	4.53	3.08	2.90	2.99
FeO	16.70	17.71	17.38	17.47	17.30	17.66	18.12	17.48	17.87	16.93
Fe_2O_3	3.28	3.74	3.41	3.43	3.39	3.46	3.55	3.43	3.50	3.32
MnO	0.12	0.16	0.23	0.14	0.11	0.22	0.26	0.23	0.20	0.31
MgO	7.87	7.66	7.63	8.12	6.94	7.77	6.70	7.70	7.73	8.03
CaO	0.00	0.12	0.01	0.00	0.11	0.00	0.01	0.00	0.03	0.04
Na_2O	0.12	0.14	0.16	0.12	0.12	0.27	0.19	0.21	0.14	0.27
K_2O	9.10	8.61	9.07	8.92	8.87	9.26	9.41	9.40	9.31	9.24
Total	95.93	94.99	95.38	95.37	95.50	95.25	95.68	95.37	95.19	95.18
Si	2.68	2.64	2.64	2.65	2.64	2.63	2.60	2.65	2.63	2.65
Al^{IV}	1.32	1.36	1.36	1.35	1.36	1.37	1.40	1.35	1.37	1.35
Al^{VI}	0.37	0.31	0.33	0.33	0.30	0.37	0.30	0.37	0.36	0.37
Ti	0.23	0.22	0.22	0.20	0.30	0.17	0.26	0.18	0.17	0.17
Fe^{2+}	1.05	1.14	1.11	1.11	1.10	1.13	1.16	1.12	1.14	1.08
Fe^{3+}	0.19	0.20	0.20	0.20	0.19	0.20	0.20	0.20	0.20	0.19
Mn	0.01	0.01	0.02	0.01	0.01	0.01	0.02	0.02	0.01	0.02
Mg	0.88	0.87	0.87	0.92	0.79	0.89	0.76	0.88	0.88	0.91
Ca	0.00	0.01	0.00	0.00	0.01	0.00	0.00	0.00	0.00	0.03
Na	0.02	0.02	0.02	0.02	0.02	0.04	0.03	0.03	0.02	0.04
K	0.87	0.84	0.88	0.86	0.86	0.90	0.92	0.91	0.91	0.90
Total	7.62	7.62	7.65	7.65	7.58	7.71	7.65	7.71	7.69	7.71

Cations calculated on the basis of 11 oxygens assuming a fixed ratio of $Fe^{3+}/Fe_{tot} = 0.15$. meso, mesosome; leuco, leucosome.

The solidus temperature for similar migmatites from the Schwarzwald was determined from melting experiments under water-saturated conditions (Mehnert & Büsch, 1982). The authors reported temperatures of 675–690° C at pressures of 0.4 GPa. The same temperatures were independently constrained from two-feldspar thermometry (Stormer & Whitney, 1977) by these authors. Solidus temperatures for Qtz–Ab–An–Or–systems have been experimentally determined. The results of Johannes (1978, 1985) give water-saturated solidus temperatures of 690° C for plagioclase compositions of An_{20} at 0.5 GPa and of 740° C for the same system at 0.2 GPa (Johannes, 1989). Experiments with variable a_{H_2O} at 0.5 and at 1.0 GPa (see Johannes & Holtz, 1990) or without an additional fluid phase at 1.5 GPa (Huang & Wyllie, 1975, using natural muscovite granite and tonalite as starting materials), show increasing solidus temperatures, ranging from water-saturated solidus temperatures to more than 1100° C for vapour-free systems.

Since biotite was present during migmatization, the maximum temperatures experienced by the samples are constrained by fluid-absent melting of biotite in the presence of plagioclase, quartz, and an Al_2SiO_5-phase. For the pressure range 0.4–0.7 GPa, the reaction bt + pl + als + qtz = l + grt ± kfs is between 740 and 790° C (Le Breton & Thompson, 1988). Thus, the implication of the experimental results is that temperatures were between 675 and 740° C during stage 3 (migmatite formation).

ISOTOPE STUDIES

Element concentrations, isotope ratios, ages, and respective errors are shown in Table 2 (U–Pb data) and Table 3 (Rb–Sr data). Analytical procedures are described in the Appendix.

U–Pb dating on monazites

Pb analyses on monazites from four migmatite samples (including sample Zas-1) and from four non-migmatitic gneisses yielded concordant or quasi-concordant ages between 333 and 330 Ma (see Fig. 4 and Table 2).

Being concordant, the obtained ages must reflect either crystallization of the monazites or complete resetting of their U–Pb systems during Variscan metamorphism. The possibility of complete resetting can be tested by comparing the *P–T* conditions for the studied rocks with experimentally derived or calculated closure temperatures. The problems with this approach are the lack of experimental data on the U–Pb system in monazites and the dependence of calculated closure temperatures on parameters such as grain size, fluids, and cooling rate which are generally neither accessible nor comparable. Therefore, only empirical estimations of the closure temperatures for U and Pb in monazites are available which are based on (1) the preservation of inherited monazites in leucogranites with calculated temperature

Table 2. Results of U–Pb analyses on monazites.

Sample number and rock type*	Sample weight (mg)	Measured ratios**			Calculated ratios***		Concentrations			Apparent ages		
		$^{208}Pb/^{206}Pb$	$^{207}Pb/^{206}Pb$	$^{204}Pb/^{206}Pb$	$^{206}Pb/^{238}U$	$^{207}Pb/^{235}U$	U (ppm)	Pb (ppm)	Pb_{com} (ppm)	$^{206}Pb/^{238}U$	$^{207}Pb/^{235}U$	$^{207}Pb/^{206}Pb$
Wa 1: migmatite, (qtz, pl, kfs, bt, grt crd, sil, ap, zrn, mnz)	0.875	2.35042 ±0.00035	0.054933 ±0.000029	0.000132 ±0.000025	0.052579 ±0.000050	0.38426 ±0.00137	5022	779	1.80	330.3 ±0.6	330.2 ±1.6	329.0
Zas-1: migmatite (qtz, pl, kfs, bt, sil,ms, ap, zrn, grt, mnz)	0.828	2.76417 ±0.00052	0.055051 ±0.000022	0.000138 ±0.000013	0.052645 ±0.000034	0.38495 ±0.00077	5024	876	1.90	330.7 ±0.4	330.7 ±1.2	330.2
T 129: migmatite (qtz, pl, kfs, bt, ap, zrn, mnz)	2.302	4.40478 ±0.00055	0.054430 ±0.000012	0.000086 ±0.000004	0.052545 ±0.000131	0.38521 ±0.00099	5080	1263	1.26	330.1 ±1.6	330.9 ±1.4	336.0
Z 49: migmatitic vein (qtz, pl, kfs, bt, ms, crn, spl, ky, sil, ap, zrn, mnz)	1.356	1.59988 ±0.00012	0.056494 ±0.000003	0.000245 ±0.000006	0.052486 ±0.000023	0.38287 ±0.00048	4837	585	3.72	329.8 ±0.4	329.1 ±1.2	324.8
Al 1: gneiss (qtz, pl, kfs, grt, crd, sil, ap, zrn, mnz)	2.444	5.05059 ±0.00072	0.055243 ±0.000013	0.000145 ±0.000009	0.052448 ±0.000055	0.38417 ±0.00069	3849	1070	1.67	329.5 ±0.6	330.1 ±1.0	334.1
O 3: gneiss (qtz, pl, kfs, grt, bt, hbl, ap, zrn, mnz)	2.481	3.25567 ±0.00050	0.053738 ±0.000007	0.000052 ±0.000009	0.053080 ±0.000134	0.38776 ±0.00113	5323	1054	0.80	333.4 ±1.6	332.7 ±1.6	328.0
S 7: gneiss (qtz, pl, bt, hbl, ttn, ap, zrn, mnz)	1.903	2.33934 ±0.00034	0.054299 ±0.000006	0.000086 ±0.000004	0.052851 ±0.000025	0.38650 ±0.00031	5534	860	1.44	332.0 ±0.4	331.8 ±0.4	330.5
We 1: gneiss (qtz, pl, kfs, bt, hbl, ap, zrn, mnz)	1.243	1.52857 ±0.00020	0.058312 ±0.000024	0.000365 ±0.00002	0.052913 ±0.000150	0.38641 ±0.00012	5868	698	6.71	332.4 ±1.4	331.8 ±1.1	327.3

*In all samples monazite occurs in the biotite-rich parts of the rocks and very often forms inclusions in biotite. Abbreviations for minerals are: ap: apatite, bt: biotite, crd: cordierite, crn: corundum, grt: garnet, hbl: hornblende, kfs: K-feldspar, ky: kyanite, mnz: monazite, ms: muscovite, pl: plagioclase, qtz: quartz, sil: sillimanite, spl: spinel, ttn: titanite, zrn: zircon. **Measured ratios (no corrections for blank and spike) from IC run (see Appendix); the indicated errors are 2σ errors. ***Errors were calculated according to the procedure of Ludwig (1980). Pb_{com}, common lead.

constraints, (2) closed-system behaviour of monazites formed at staurolite-grade conditions during later sillimanite-grade metamorphism (Smith & Barreiro, 1990), and (3) the inferred resetting of U and Pb in monazites at granulite facies conditions (Machado *et al.*, 1989). All these studies suggest closure temperatures of 700–730° C which is within the upper temperature range inferred for the migmatites of this study.

Nevertheless, overstepping of the specific closure temperature does not necessarily lead to complete resetting. In most cases the U–Pb systems of monazites lose only part of their Pb which results in discordant U–Pb ages (Black *et al.*, 1984; Teufel, 1988; Copeland *et al.*, 1988; Kingsbury *et al.*, 1990). Temperatures at which complete resetting might occur tend to exceed those of monazite stability (compare Montel, 1986; Rapp & Watson, 1986 and Kingsbury *et al.*, 1990, see Parrish, 1990). Thus, the obtained U–Pb ages on monazites are probably crystallization ages rather than ages of resetting.

Rb–Sr isochron ages and Sr profiles

Figures 5c & 6c show Rb–Sr isochron diagrams for the two migmatite samples Zas-1 and Hec-2. Each point in the diagrams corresponds to the isotopic composition of a distinct leucosome or mesosome slab. Best fit lines indicate ages of 336 ± 14 Ma for sample Hec-2 and of 329 ± 10 Ma for sample Zas-1, thus confirming the Carboniferous metamorphic event already constrained by the U–Pb data on monazites. Nevertheless, the scatter of data points along the two best fit lines points to only incomplete isotopic resetting or homogenization during the inferred metamorphic event, more clearly revealed by the Sr profile diagrams (Figs 5b & 6b).

In contrast to the conventional isochron diagrams, the presentation of back-calculated Sr data in profile diagrams reveals further information on the degree and nature of isotopic resetting during metamorphism (Bachmann *et al.*, 1986). For this purpose, $^{87}Sr/^{86}Sr$ ratios are calculated back to different times, and plotted against distances, i.e. slab centres within the profiles. Connecting the points for contemporaneous Sr isotopic compositions from all slabs leads to more or less zigzag-shaped lines. The lines become continuously smoother closer to the time of isotopic resetting. Complete isotopic equilibration or homogenization throughout the profile is shown by a straight horizontal line. If homogenization was never complete, the smoothest line corresponds to the time of best-approximated isotopic homogeneity, the degree of isotopic disequilibrium being expressed by the differences in $^{87}Sr/^{86}Sr$ between adjacent slabs.

The time of best-approximated homogeneity (the smoothest line) is defined by minimum differences in $^{87}Sr/^{86}Sr$ ratios of adjacent slabs and by the constraint that any calculated isotope profile in which slabs with higher $^{87}Rb/^{86}Sr$ ratios than their neighbouring slabs show lower $^{87}Sr/^{86}Sr$ ratios is merely a fictitious isotope distribution. By comparing back-calculated $^{87}Sr/^{86}Sr$ isotope ratios of single slabs with their textures and compositions, the causes for isotopic disequilibrium may be found. Preconditions for Sr recalculations are (1) a significant spread in $^{87}Rb/^{86}Sr$ ratios throughout the studied profile,

Table 3. Results of Rb–Sr thin slab analyses.

Sample	Slab no.	Concentrations		Isotope ratios	
		Rb (ppm)	Sr (ppm)	$^{87}Rb/^{86}Sr$	$^{87}Sr/^{86}Sr$
Hec–2					
ML	1	87.4	144.0	1.7579	0.72499 ± 12**
L	2	47.2	217.8	0.6271	0.71922 ± 15**
M	3	152.7	185.3	2.3896	0.72778 ± 14**
M	4	96.2	173.3	1.6079	0.72396 ± 18**
M	5	136.4	171.4	2.3076	0.72727 ± 18**
M	6	161.1	199.8	2.3379	0.72768 ± 18**
LM	7	33.3	235.8	0.4095	0.71836 ± 17**
LM	8	58.2	196.4	0.8588	0.72034 ± 19**
L	9	44.2	239.4	0.5352	0.71885 ± 16**
M	10	127.5	220.9	1.6734	0.72460 ± 29**
ML	11	68.4	231.0	0.8576	0.72066 ± 26**
M	12	215.7	199.4	3.1371	0.73116 ± 29**
M	13	151.6	204.6	2.1478	0.72658 ± 31**
L	14	46.4	243.6	0.5515	0.71859 ± 15**
M	15	121.2	188.8	1.8592	0.72498 ± 22**
M	16	123.9	185.0	1.9403	0.72519 ± 20**
M	17	86.6	224.0	1.1205	0.72087 ± 17**
MM	18	224.9	171.1	4.1184	0.73532 ± 21**
SRM 987					0.710269 ± 23**
Zas–1					
M	1	80.2	245.0	0.9487	0.71883 ± 8*
M	2	111.1	192.0	1.6770	0.72228 ± 8*
ML	3	43.2	310.4	0.3491	0.71620 ± 8*
L	4	35.5	342.2	0.3008	0.71565 ± 8*
L	4R	35.5	342.2	0.3003	0.71565 ± 8*
ML	5	55.7	302.6	0.5331	0.71698 ± 10*
ML	5R	55.5	302.4	0.5408	0.71699 ± 6*
M	6	91.9	194.7	1.3668	0.72059 ± 6*
M	7	107.7	247.8	1.2593	0.72034 ± 7*
MM	8	168.1	117.3	4.1561	0.73379 ± 3*
SRM 987					0.710276 ± 9*

**Isotope analyses performed on Teledyne mass spectrometer.* Isotope analyses performed on VG mass spectrometer. R, complete replicate analyses; L, leucosome; LM, mixture of leucosome and minor mesosome; M, mesosome; ML, mixture of mesosome and minor leucosome; MM, melanosome.

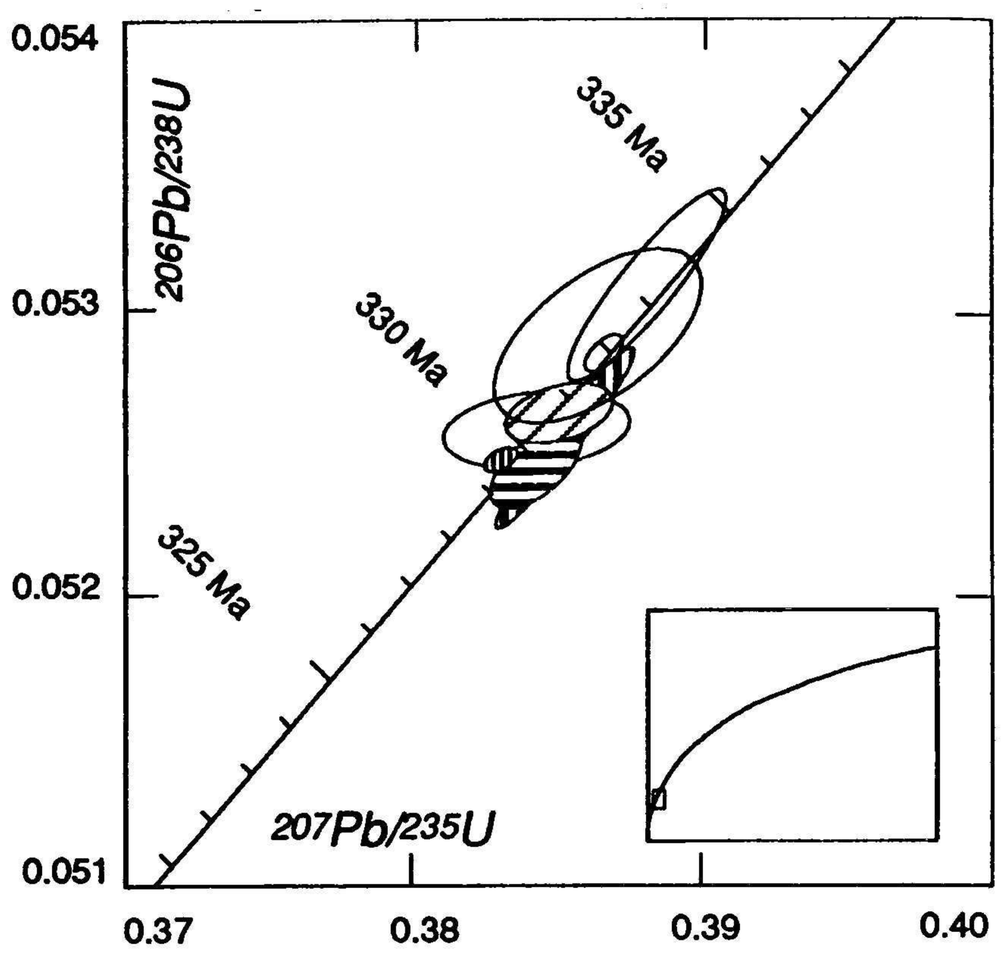

Fig. 4. Detail of the U–Pb concordia plot, showing the data points for analysed monazite fractions. Inset: the position of the detail within the concordia diagram. The error ellipses were calculated according to the procedure of Ludwig (1980). Filled symbols represent data points for monazites from migmatites, empty symbols correspond to those for non-migmatitic gneisses.

(2) simple geometric relationships between the slabs and (3) closed-system behaviour of Rb and Sr on the scale considered.

The Sr profile diagrams for the studied samples (Figs 5b & 6b) reveal two features. (1) Isotopic resetting was either not complete or disturbed by open-system behaviour affecting Rb and Sr as there is no straight horizontal line corresponding to isotopic equilibrium. (2) Assuming closed-system behaviour for Rb and Sr, the best approximation to isotopic homogeneity was achieved at the times recorded by the two best-fit lines (Figs 5c & 6c), respectively. Relating the data points for 330 Ma (Zas-1) and 335 Ma (Hec-2) in the Sr profile diagrams (Figs 5b & 6b) to the corresponding slab compositions shows that there is no strictly systematic relationship between $^{87}Sr/^{86}Sr$ ratios and the slab lithologies. In most cases low $^{87}Sr/^{86}Sr$ ratios correspond to leucosomes (slab 4 in sample Zas-1, slabs 2, 8, 9, 14 in sample Hec-2), while high $^{87}Sr/^{86}Sr$ ratios coincide with mesosomes, but there are also clear exceptions to this correlation (slab 6 in sample Zas-1, slab 12 in sample Hec-2).

DISCUSSION

The fact that monazites from gneisses and from migmatites yield the same ages shows that (1) gneisses and migmatites were formed during the same low-pressure high-temperature event in the Carboniferous, and (2) there is no major gap between the formation of the gneissose foliation (D3) and the migmatitic overprint (D4).

A Carboniferous low-temperature high-pressure event is further supported by the Rb–Sr data. The question arises as to what causes the observed Sr isotope disequilibrium patterns. Possible explanations are (1) the preservation of premetamorphic or premigmatitic Sr isotope heterogeneities due to incomplete resetting during migmatite formation, and (2) disturbance of the Rb–Sr system by synmetamorphic fluids or by retrograde hydration.

Causes of Sr isotope disequilibrium

Textural observations and the results of monazite dating on the studied rocks as well as structural evidence (Flöttmann & Kleinschmidt, 1989) suggest that migmatization overprinted a slightly older gneiss foliation. The precursor rocks to the gneisses in turn were greywackes, pelites and related sediments (Müller, 1989). As the sediments and gneisses both had a pronounced compositional banding, isotopic equilibrium was most likely never attained at a premigmatitic stage. The idea of incomplete isotope resetting during migmatite formation is supported by the observation that low $^{87}Sr/^{86}Sr$ ratios correspond

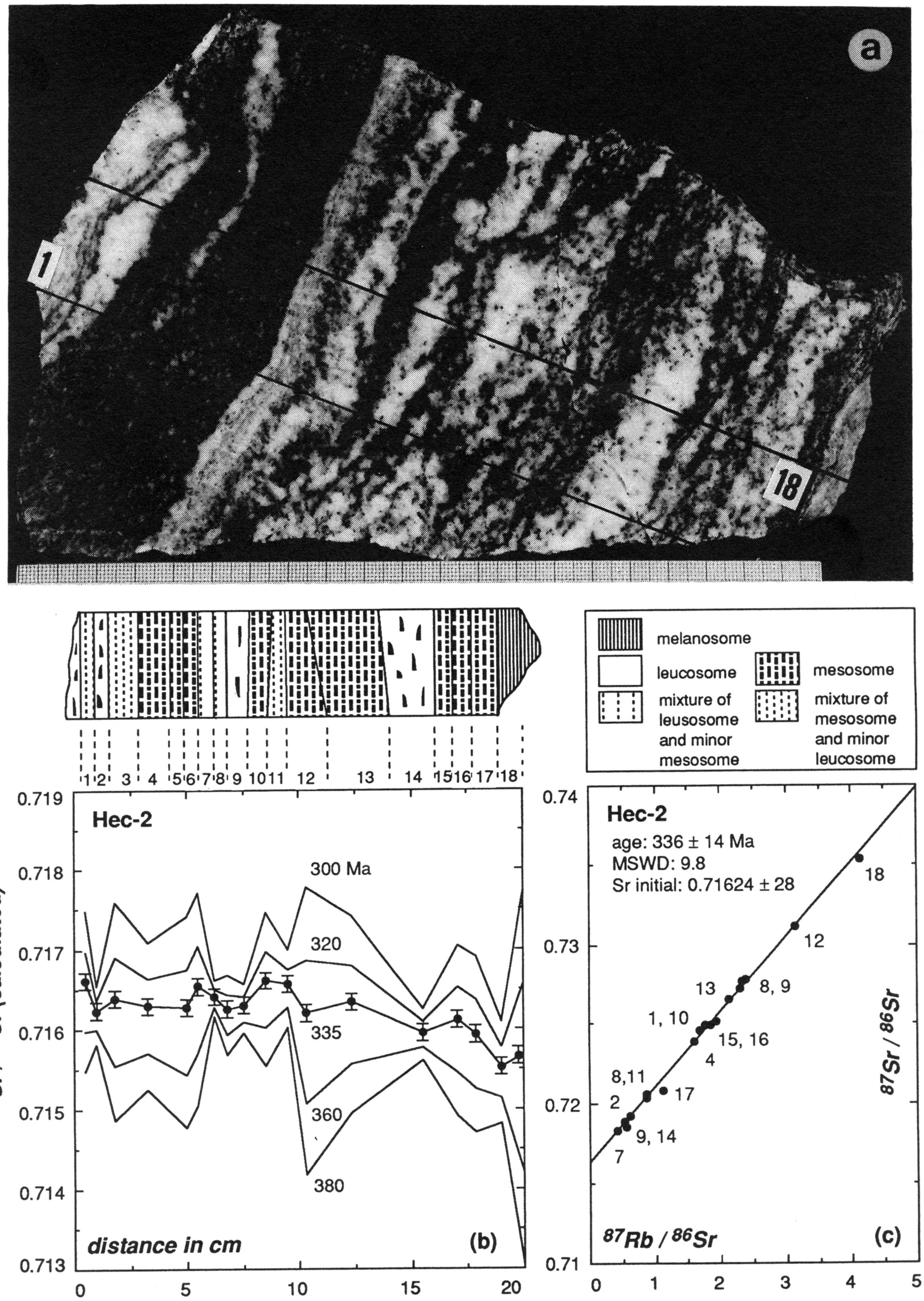

Fig. 5. (a) Photograph of migmatite sample Zas-1 with the position of the Rb–Sr thin-slab profile indicated. (b) Sr profile diagram for sample Zas-1, showing $^{87}Sr/^{86}Sr$ ratios for the single slabs calculated back to different times in the past and plotted against their distances. The schematic profile detail shown above the diagram corresponds to the profile indicated in (a). For slabs 4 and 5, the recalculated $^{87}Sr/^{86}Sr$ ratios for complete replicate analyses are also plotted (compare Table 3). For further explanation and calculation procedure see text. (c) Rb–Sr isochron diagram showing the data points for all thin slabs of profile Zas-1. The inserted numbers correspond to the slab numbers.

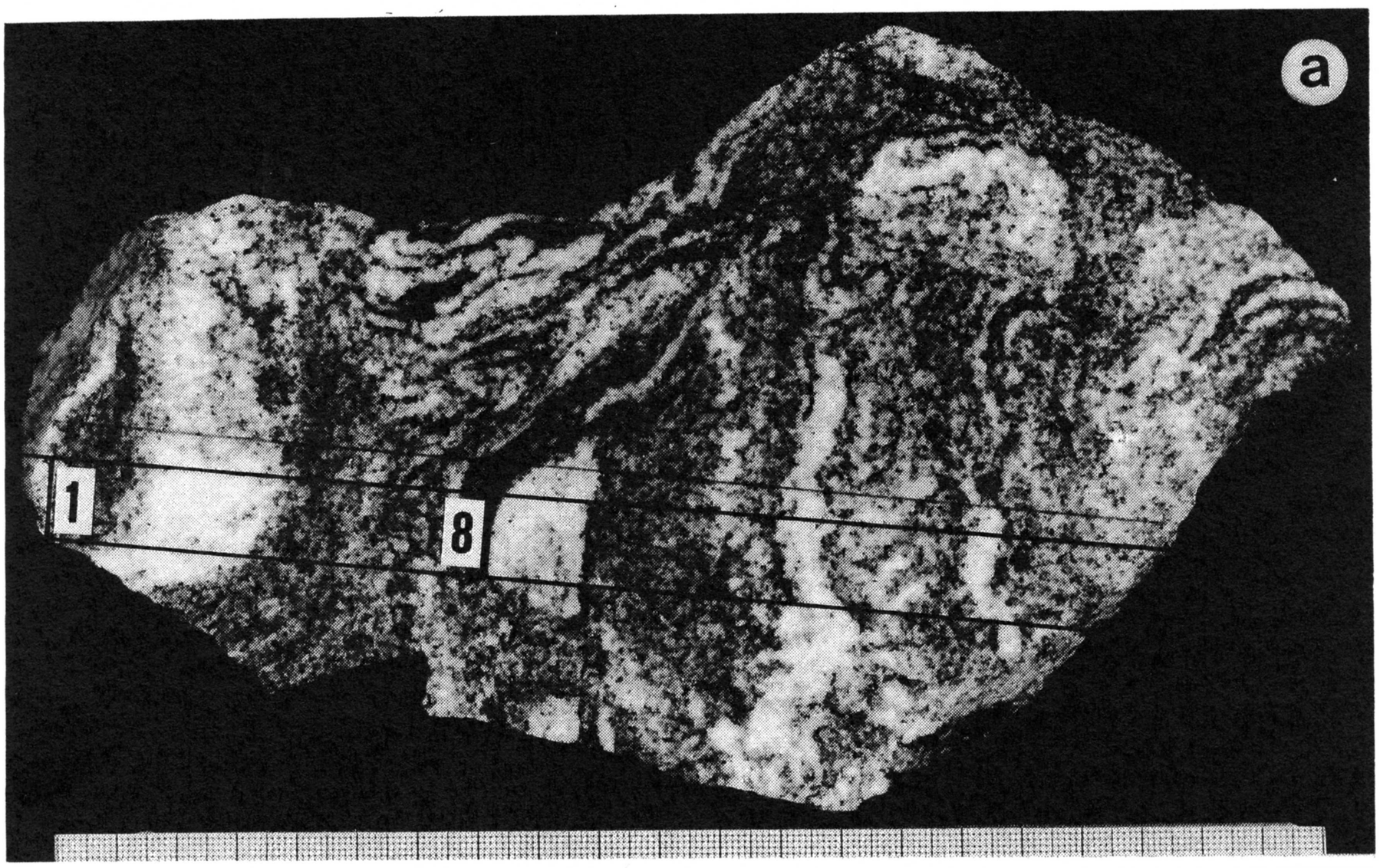

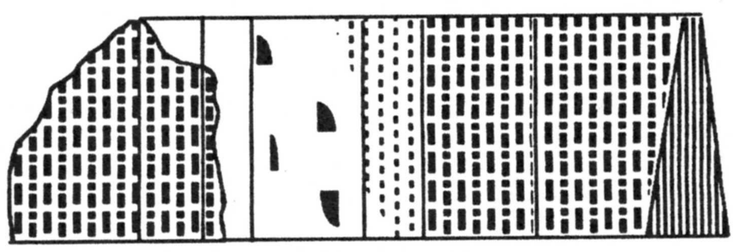

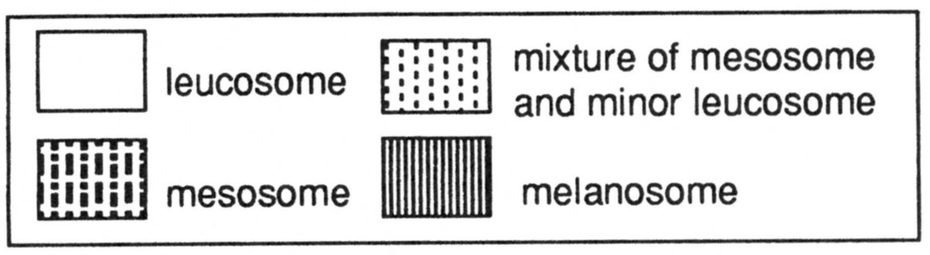

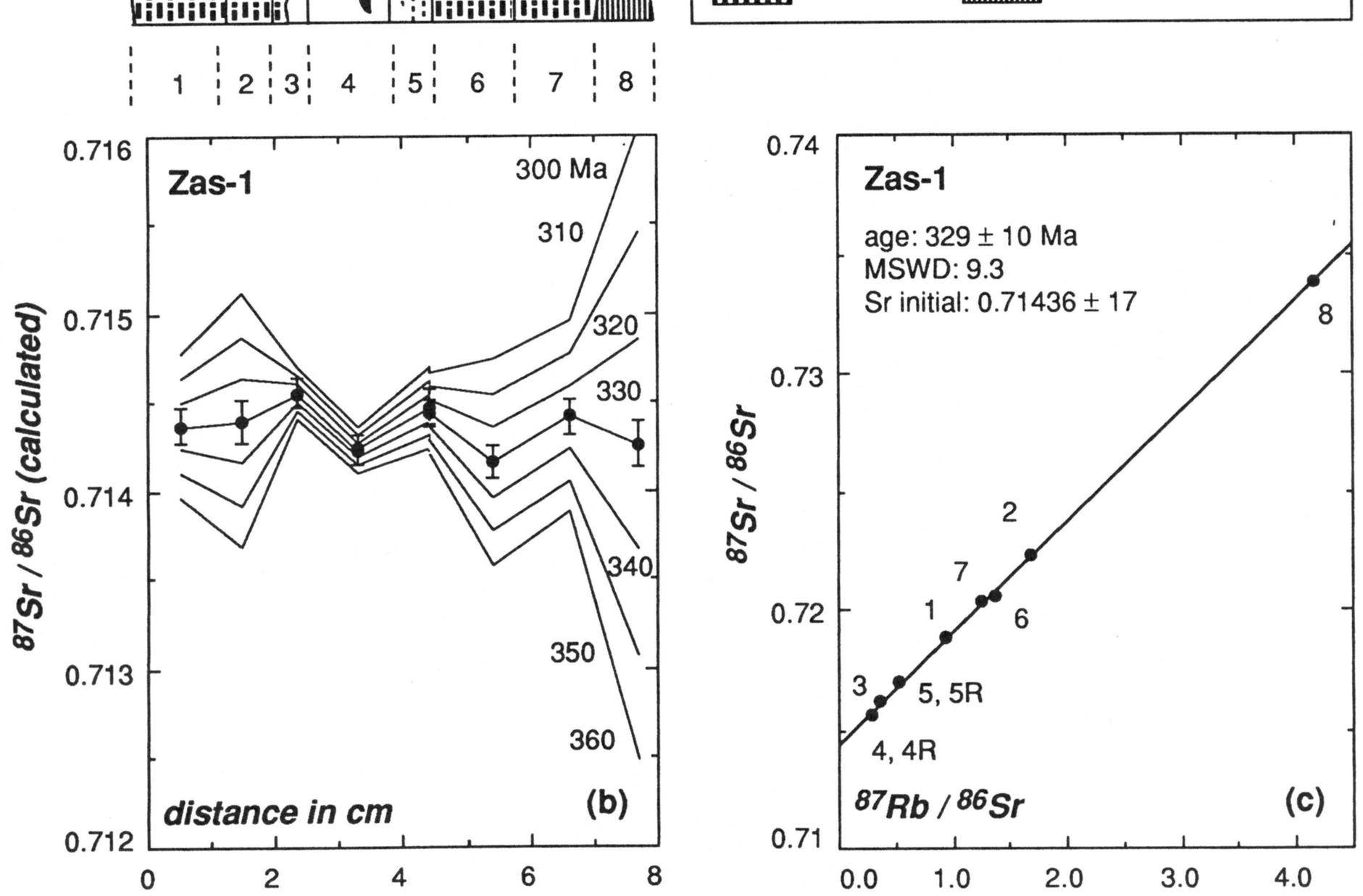

Fig. 6. (a) Photograph of migmatite sample Hec-2 with the position of the Rb–Sr thin-slab profile indicated. (b) Sr profile diagram for sample Hec-2, showing $^{87}Sr/^{86}Sr$ ratios for the single slabs calculated back to different times in the past and plotted against their distances. The schematic profile shown above the diagram corresponds to the profile indicated in (a). For further explanation and calculation procedure see text. (c) Rb–Sr isochron diagram showing the data points for all thin slabs of profile Hec-2. The inserted numbers correspond to the slab numbers.

mainly with leucosomes while high $^{87}Sr/^{86}Sr$ ratios coincide with mesosomes. This correlation is due to the fact that mesosomes are enriched in biotite which has a high Rb/Sr ratio and thus accumulates radiogenic ^{87}Sr preferentially. Leucosomes are depleted in biotite and enriched in plagioclase which strongly incorporates Sr.

The idea of incomplete homogenization of isotopes is further corroborated by the nature of the processes involved in migmatite formation. Partial melting as a process that strongly enhances volume interdiffusion and thus isotope exchange played virtually no role during migmatite formation. The mechanisms responsible for element exchange in the studied rocks are probably diffusive mass transfer and dislocation creep. Although deformation can enhance element exchange rates between grains, the study of McCaig & Knipe (1990) and the experiments of Yund & Tullis (1991) have shown that chemical equilibrium on grain scale and in small rock volumes was not attained during deformation at high temperatures.

Comparable results have been obtained on banded migmatites from northern Switzerland. On the basis of oxygen isotope studies, Mazurek (1992) concluded that oxygen isotope fractionation between mineral phases of subsolidus amphibolite facies assemblages were only partly disturbed by later partial melting. From mineral and textural data, Mazurek (1992) also deduced that melt fractions were rather small. These findings are also supported by recent experimental determinations of Sr diffusion coefficients in feldspars as well as by calculated closure temperatures for Sr in feldspars (Giletti, 1991; Cherniak & Watson, 1992). They show Sr diffusion in feldspars to be very slow and closure temperatures to be rather high, thus requiring extended periods of high-temperature metamorphism for complete homogenization.

The second possible cause of isotopic disequilibrium is open-system behaviour of Rb and Sr, enhanced by fluid infiltration during migmatization, which is merely a special case of incomplete resetting as discussed above. The presence of fluids during high-temperature metamorphism cannot be constrained from textures and mineral compositions but is suggested by non-symmetrical zoning in plagioclase grains (McCaig & Knipe, 1990) and by the presence of myrmekite (Phillips, 1980).

Hydrothermal alteration of the samples is documented by partial alteration of plagioclase to sericite and by partial hydration of biotite to chlorite. Hydrothermal alteration is quite common in the basement of the Schwarzwald as deduced mainly from stable isotope studies (Hoefs & Emmermann, 1983; Simon & Hoefs, 1987; Simon, 1990; Mazurek, 1992). The retrograde hydration reactions have been ascribed to circulating fluids of meteoric origin (Hoefs & Emmermann, 1983). Sericite growth at the expense of plagioclase in amphibolites from the Schwarzwald took place in Mesozoic times (150–110 Ma) as indicated by $^{40}Ar/^{39}Ar$ dating results (Kirsch, 1989). The formation of sericite from plagioclase involves loss of Na^+ and Ca^{2+} and addition of K^+ and is therefore likely to change the $^{87}Rb/^{86}Sr$ ratios by addition of Rb.

For the studied profiles, an increase of $^{87}Rb/^{86}Sr$ ratios during hydrothermal alteration at 110–150 Ma would significantly affect the plagioclase-rich leucosomes. Calculating their $^{87}Sr/^{86}Sr$ ratios for 330 Ma on the basis of $^{87}Rb/^{86}Sr$ ratios that are too high would lead to an anomalously rapid decrease of $^{87}Sr/^{86}Sr$ ratios with time. This effect is consistent with the low $^{87}Sr/^{86}Sr$ ratios of most of the leucosomes at 330 Ma (Zas-1) and at 335 Ma (Hec-2) compared with the mesosomes. Nevertheless, sericite growth is thought to have had only minor effects on Sr isotope redistribution as it is not very pronounced in the studied samples and as leucosomes still have consistently very much lower $^{87}Rb/^{86}Sr$ ratios than mesosomes (Table 3).

In conclusion, the best approximation to Sr isotope equilibrium was attained during high-temperature metamorphism. Disequilibrium most likely resulted from the preservation of premigmatitic Sr isotope patterns in conjunction with a lack of resetting during metamorphic segregation processes. Retrograde hydration obviously caused no significant shift in Sr isotope distributions but its influence cannot be eliminated.

Geological implications

In the basement rocks of the Schwarzwald, textures and mineral compositions (see above) indicate that stromatic migmatites of psammitic compositions were probably generated by metamorphic segregation processes at subsolidus conditions and not by partial melting. Nevertheless, the presence of very small amounts of melt in these rocks during migmatization is not excluded and it must be stressed that non-stromatic migmatites and migmatites of other compositions may very well have formed by partial melting.

The geochronological results link low-pressure high-temperature metamorphism in the Schwarzwald to the intrusion of granitoid magmas, dated between 340 and 310 Ma. They also allow for a geochronological correlation of the Schwarzwald with other Moldanubian areas, where low-pressure high-temperature metamorphism took place largely between 340 and 310 Ma (Grauert *et al.*, 1974; Teufel, 1988; Kreuzer *et al.*, 1989 for the Bohemian Massif; Montigny & Thuizat, 1989 for the Vosges Mountains; Pin & Peucat, 1986 for the Armorican Massif and the Massif Central).

General implications for migmatite dating

Most migmatites are chemically, texturally and isotopically markedly heterogeneous on a comparatively small scale (see Bickle *et al.*, 1988). The possibility that high-temperature metamorphism may fail to equilibrate Sr isotopes even on a small scale, as demonstrated in this case, implies that Rb–Sr conventional whole rock dating on large non-homogeneous rock samples may fail to detect migmatite formation as the use of isochron diagrams requires complete isotopic resetting throughout the

sampled areas. This is clearly demonstrated by examples of conventional Rb–Sr whole rock dating on Variscan migmatites and gneisses (Hofmann & Köhler, 1973; Köhler & Müller-Sohnius, 1980, 1985; Bickle *et al.*, 1988). The strong scatter of data points in the corresponding isochron diagrams point to an Ordovician age in all the cases, although migmatization is clearly of Carboniferous age. Additionally, the large sample sizes preclude petrological constraints on the dating results.

Sr thin-slab profiles, on the other hand, serve to illustrate the scatter in $^{87}Sr/^{86}Sr$ ratios quite well. As sample sizes are small, petrological control on migmatite-forming processes is possible and may help to explain the isotope patterns. Rb–Sr thin-slab dating may also record metamorphic events that did not result in complete isotopic resetting.

CONCLUSIONS

Rb–Sr thin-slab dating as well as microprobe analyses of mineral phases have been carried out on two centimetre-scale migmatite profiles from the Schwarzwald. Together with the results of U–Pb isotope analyses of monazites from migmatites and from non-migmatitic gneisses, they allow the following conclusions to be made.

1 In the Schwarzwald, gneisses and migmatites were generated during one single high-temperature event in the Carboniferous (335–330 Ma).

2 Textures and phase compositions provide no evidence of partial melting and suggest that metamorphic segregation processes (deformation-enhanced mass transport) produced the migmatitic textures and the phase compositions. They also point to small-scale chemical disequilibrium during migmatization.

3 Sr disequilibrium patterns in two migmatite profiles are most likely due to a lack of isotopic equilibration during migmatite formation. They may have partially been influenced by Mesozoic sericite formation.

4 The results also impose limitations on the validity of conventional whole rock dating in determining migmatite formation ages and demonstrate the necessity of combining isotope studies with textural and microchemical information.

ACKNOWLEDGEMENTS

We thank H.-P. Meyer for help with the microprobe work and H. Baier for sample preparation. We also thank R. Altherr for critical comments on the manuscript and for discussions which helped to clarify several of the ideas presented in this paper. Constructive reviews by J. S. Daly and an anonymous reviewer are gratefully acknowledged. This paper is a contribution within the research program 'Orogene Prozesse – ihre Quantifizierung und Simulation am Beispiel der Varisziden' funded by the Deutsche Forschungsgemeinschaft which also provided financial support for isotope analyses.

REFERENCES

Ashworth, J. R., 1985. Introduction. In: *Migmatites* (ed. Ashworth, R.), pp. 1–35. Blackie, Glasgow.

Bachmann, G., Grauert, B. & Miller, H., 1986. Isotopic dating of polymetamorphic metasediments from northwest Argentinia. *Zentralblatt für Geologie und Paläontologie*, **Teil I** (1985), 1257–1268.

Barbey, P., Bertrand, J.-M., Angoua, S. & Dautel, D., 1989. Petrology and U/Pb geochronology of the Telohat migmatites, Aleksod, Central Hoggar, Algeria. *Contributions to Mineralogy and Petrology*, **101,** 207–219.

Bickle, M. J., Wickham, S. M., Chapman, H. J. & Taylor, Jr, H. P., 1988. A strontium, neodymium and oxygen isotope study of hydrothermal metamorphism and crustal anatexis in the Trois Seigneurs Massif, Pyrenees, France. *Contributions to Mineralogy and Petrology*, **100,** 399–417.

Black, L. P., Fitzgerald, J. D. & Harley, S. L., 1984. Pb isotopic composition, colour and microstructure of monazites from a polymetamorphic rock in Antarctica. *Contributions to Mineralogy and Petrology*, **85,** 141–148.

Brewer, M. S. & Lippolt, H. J., 1974. Petrogenesis of basement rocks of the Upper Rhine Region elucidated by rubidium–strontium systematics. *Contributions to Mineralogy and Petrology*, **45,** 123–141.

Cherniak, D. J. & Watson, E. B., 1992. A study of strontium diffusion in K-feldspar, Na–K-feldspar and anorthite using Rutherford Backscattering Spectroscopy. *Earth and Planetary Science Letters*, **113,** 411–425.

Clemens, J. D. & Vielzeuf, D., 1987. Constraints on melting and magma production in the crust. *Earth and Planetary Science Letters*, **86,** 287–306.

Conrad, W. K., Nicholls, I. A. & Wall, V. J., 1988. Water-saturated and undersaturated melting of metaluminous and peraluminous crustal compositions at 10 kb, evidence for the origin of silicic magmas in the Taupo Volcanic Zone, New Zealand, and other occurrences. *Journal of Petrology*, **29(4),** 765–803.

Copeland, P., Parrish, R. R. & Harrison, T. M., 1988. Identification of inherited radiogenic Pb in monazite and implications for U-Pb systematics. *Nature*, **333,** 760–763.

Echtler, H. P & Chauvet, A., 1991/92. Carboniferous convergence and subsequent crustal extension in the Southern Schwarzwald (SW Germany). *Geodinamica Acta*, **5,** 37–49.

Eisbacher, G. H., Lüschen, E. & Wickert, F., 1989. Thrusting and Extension in the Hercynian. *Tectonics*, **8,** 1–21.

Flöttmann, T. & Kleinschmidt, G., 1989. Structural and basement evolution in the Central Schwarzwald Gneiss Complex. In: *The German Continental Deep Drilling Program (KTB)* (eds Emmermann, R. & Wohlenberg, J.), pp. 265–275. Springer, Berlin.

Giletti, B. J., 1991. Rb and Sr diffusion in alkali feldspars, with implications for the cooling histories of rocks. *Geochimica et Cosmochimica Acta*, **55,** 1331–1343.

Grauert, B., Hänny, R. & Soptranajova, G., 1974. Geochronology of a polymetamorphic and anatectic gneiss region: the Moldanubicum of the Area Lam-Deggendorf, eastern Bavaria, Germany. *Contributions to Mineralogy and Petrology*, **45,** 37–63.

Hoefs, J. & Emmermann, R., 1983. The oxygen isotope composition of Hercynian granites and Pre-Hercynian gneisses from the Schwarzwald, Germany. *Contributions to Mineralogy and Petrology*, **83,** 320–329.

Hofmann, A. & Köhler, H., 1973. Whole-rock Rb–Sr-ages of anatectic gneisses from the Schwarzwald, SW-Germany. *Neues Jahrbuch für Mineralogie, Abhandlungen*. **119(2),** 1–27.

Holtz, F. & Johannes, W., 1991. Genesis of peraluminous granites I. Experimental investigation of melt compositions at 3 and 5 kb and various H2O activities. *Journal of Petrology*, **32(5),** 935–958.

Hradetzky, H., 1989. Untersuchungen zur prävariskischen

geologischen Entwicklung des zentralen Schwarzwaldes. *Unpubl. PhD Thesis, University of Heidelberg*.

Huang, W. L. & Wyllie, P. J., 1975. Melting reactions in the system NaAlSi3O8 – KAlSi3O8 – SiO2 to 35 kbars, dry and with excess water. *Journal of Geology*, **83,** 737–748.

Johannes, W., 1978. Melting of plagioclase in the system Ab–An–H_2O and Qz–Ab–An–H_2O at 5 kbars, an equilibrium problem. *Contributions to Mineralogy and Petrology*, **66,** 295–303.

Johannes, W., 1985. The significance of experimental studies for the formation of migmatites. In: *Migmatites* (ed. Ashworth, J. R.), pp. 36–85. Blackie, London.

Johannes, W., 1989. Melting of plagioclase-quartz assemblages at 2 kbar water pressure. *Contributions to Mineralogy and Petrology*, **103,** 270–276.

Johannes, W. & Gupta, L.N., 1982. Origin and evolution of a migmatite. *Contributions to Mineralogy and Petrology*, **79,** 114–123.

Johannes, W. & Holtz, F., 1990. Formation and composition of H2O-undersaturated granitic melts. In: *High-temperature Metamorphism and Crustal Anatexis* (eds Ashworth, J. R. & Brown, M.), pp. 87–101. Unwin Hyman, London.

Kalt, A., Hanel, M., Schleicher, H. & Kramm, U., 1994. Petrology and geochronology of eclogites from the Variscan Schwarzwald (F.R.G.). *Contributions to Mineralogy and Petrology*, **115,** 287–302.

Kerrick, D. M., 1972. Experimental determination of muscovite + quartz stability with $p_{H_2O} < p_{total}$. *American Journal of Science*, **272,** 946–958.

Kingsbury, J. A., Miller, C. F., Wooden, J. L. & Harrison, T. M., 1990. Utility of monazite in geochronology, examples from the Old Woman–Piute Mountains, southeastern California. *Transactions of the American Geophysical Union*, **71(17),** 654.

Kirsch, H., 1989. $^{40}Ar/^{39}Ar$-chronologische Untersuchungen zur Sericitisierung von Plagioklasen. *Unpubl. PhD Thesis, University of Heidelberg*.

Knipe, R. J., 1989. Deformation mechanisms – recognition from natural tectonites. *Journal of Structural Geology*, **11,** 127–146.

Kober, B., 1986. Whole-grain evaporation for $^{207}Pb/^{206}Pb$-age investigations on single zircons using a double filament thermal ion source. *Contributions to Mineralogy and Petrology*, **93,** 482–490.

Kober, B., 1987. Single-zircon evaporation with Pb^+ emitter bedding using thermal ion mass spectrometry, and implications to zirconology. *Contributions to Mineralogy and Petrology*, **96,** 63–71.

Köhler, H. & Müller-Sohnius, D., 1980. Rb–Sr systematics on paragneiss series from the Bavarian Moldanibicum, Germany. *Contributions to Mineralogy and Petrology*, **71,** 387–392.

Köhler, H. & Müller-Sohnius, D., 1985. Rb–Sr Altersbestimmungen und Sr-Isotopensystematik an Gesteinen des Regensburger Waldes, (Moldanubikum NE Bayerns). *Neues Jahrbuch für Mineralogie, Abhandlungen*, **151(1),** 1–28.

Kreuzer, H., Seidel, E., Schüssler, U., Okrusch, M., Lenz, K. L. & Raschka, H., 1989. K-Ar geochronology of different tectonic units at the northwestern margin of the Bohemian Massif. *Tectonophysics*, **157,** 149–178.

Krogh, T. E., 1973. A low-contamination method for hydrothermal decomposition of zircon and extraction of U and Pb for isotope determination. *Geochimica et Cosmochimica Acta*, **37,** 485–494.

Krohe, A. & Eisbacher, G. H., 1988. Oblique crustal detachment in the Variscan Schwarzwald, southwestern Germany. *Geologische Rundschau*, **77/1,** 25–43.

Le Breton, N. & Thompson, B. A., 1988. Fluid-absent (dehydration) melting of biotite in metapelites in the early stages of crustal anatexis. *Contributions to Mineralogy and Petrology*, **99,** 226–237.

Lindh, A. & Wahlgren, C. H., 1985. Migmatite formation at subsolidus conditions – an alternative to anatexis. *Journal of Metamorphic Geology*, **3,** 1–12.

Ludwig, K. R., 1980. Calculation of uncertainties of U–Pb-isotope data. *Earth and Planetary Science Letters*, **46,** 212–220.

Machado, N, Goulet, N. & Gariépy, C., 1989. U–Pb geochronology of reactivated Archean basement and of Hudsonian metamorphism in the northern Labrador Trough. *Canadian Journal of Earth Sciences*, **26,** 1–15.

Mazurek, M., 1992. Phase equilibria and oxygen isotopes in the evolution of metapelitic migmatites, a case study from the Pre-Alpine basement of northern Switzerland. *Contributions to Mineralogy and Petrology*, **109,** 494–510.

McCaig, A. M. & Knipe, R. J., 1990. Mass transport mechanisms in deforming rocks: Recognition using microstructural and microchemical criteria. *Geology*, **18,** 824–827.

McLellan, E. L., 1983. Contrasting textures in metamorphic and anatectic migmatites: an example from the Scottish Caledonides. *Journal of Metamorphic Geology*, **1,** 241–261.

Mehnert, K. R. & Büsch, W., 1982. The initial state of migmatite formation. *Neues Jahrbuch für Mineralogie, Abhandlungen*, **145,** 211–238.

Montel, J. M., 1986. Experimental determination of the solubility of Ce-monazite in SiO_2–Al_2O_3–K_2O–Na_2O-melts at 800° C, 2 kbar, under H_2O-saturated conditions. *Geology*, **14,** 659–662.

Montigny, R. & Thuizat, R., 1989. K–Ar and $^{40}Ar^{39}Ar$ ages on crystalline rocks of the Vosges. *Terra abstracts*, **1,** 352.

Müller, H. D., 1989. Geochemistry of metasediments in the Hercynian and pre-Hercynian crust of the Schwarzwald, the Vosges and northern Switzerland. *Tectonophysics*, **157,** 97–108.

Parrish, R. R., 1990. U–Pb dating of monazite and its application to general geological problems. *Canadian Journal of Earth Sciences*, **27,** 1431–1450.

Patiño Douce, A. E. & Johnston, A. D. 1991. Phase equilibria and melt productivity in the pelitic system: implications for the origin of peraluminous granitoids and aluminous granulites. *Contributions to Mineralogy and Petrology*, **107,** 202–218.

Phillips, E. R., 1980. On polygenetic myrmekite. *Geological Magazine*, **117,** 29–36.

Pin, C. & Peucat, J. J., 1986. Ages des épisodes de mtamorphisme paléozoique dans le Massif central et le Massif Armoricain. *Bulletin de la Societé Géologique de France*, **8(3),** 461–469.

Puziewicz, J. & Johannes, W., 1990. Experimental study of a biotite-bearing granitic system under water-saturated and water-undersaturated conditions. *Contributions to Mineralogy and Petrology*, **104,** 397–406.

Rapp, R. P. & Watson E. B., 1986. Monazite solubility and dissolution kinetics: implications for the thorium and light rare earth chemistry of felsic magmas. *Contributions to Mineralogy and Petrology*, **94,** 304–316.

Rubie, D. C. & Brearley, A. J., 1990. A model for rates of disequilibrium melting during metamorphism. In: *High-Temperature Metamorphism And Crustal Anatexis* (eds Ashworth, J. R. & Brown, M.), pp. 57–84. Unwin Hyman, London.

Rutter, M. J. & Wyllie, P. J., 1988. Melting of vapour-absent tonalite at 10 kbar to simulate dehydration-melting in the deep crust. *Nature*, **331,** 159–160.

Sawyer, E. W. & Barnes, S.-J., 1988. Temporal and compositional differences between subsolidus and anatectic migmatite leucosomes from the Quetico metasedimentary belt, Canada. *Journal of Metamorphic Geology*, **6,** 437–450.

Sawyer, E. W. & Robin, P.-Y. F., 1986. The subsolidus generation of layer-parallel quartz–feldspar veins in greenschist to upper amphibolite facies metasediments. *Journal of Metamorphic Geology*, **4,** 237–260.

Simon, K., 1990. Hydrothermal alteration of Variscan granites, southern Schwarzwald, Federal Republic of Germany. *Contributions to Mineralogy and Petrology*, **105,** 177–196.

Simon, K. & Hoefs, J., 1987. Effects of meteoric water interaction on Hercynian granites from the Südschwarzwald, southwest Germany. *Contributions to Mineralogy and Petrology*, **61,** 253–261.

Skjerlie, K. P., Patino Douce, A. E. & Johnston, A. D., 1993. Fluid absent melting of a crustal protolith: implications for the

generation of anatectic granites. Contributions to Mineralogy and Petrology, 114, 365–378.
Smith, H. A. & Barreiro, B., 1990. Monazite U–Pb dating of staurolite grade metamorphism in pelitic schists. *Contributions to Mineralogy and Petrology*, **105,** 602–615.
Stacey, J. S. & Kramers, J. D., 1975. Approximation of terrestrial lead isotope evolution by a two-stage model. *Earth and Planetary Science Letters*, **26,** 207–221.
Steiger, R. H., Bär, M. T. & Büsch, W., 1973. The Zircon Age of an Anatectic Rock in the Central Schwarzwald. *Fortschritte der Mineralogie*, **50,** Beiheft, 3, 131–132.
Steiger, R. H. & Jäger, E., 1977. Subcommission on geochronology: convention on the use of decay constants in geo- and cosmochronology. *Earth and Planetary Science Letters*, **36,** 359–362.
Stormer, J. C. & Whitney, J. A., 1977. Two-feldspar geothermometry in granulite facies metamorphic rocks. *Contributions to Mineralogy and Petrology*, **65,** 123–133.
Teufel, S., 1988. Vergleichende U–Pb und Rb–Sr-Altersbestimungen an Gesteinen des Übergangsbereiches Saxothuringikum/Moldanubikum, NE-Bayern. *Göttinger Arbeiten zur Geologie und Paläontologie*, **35**.
Thompson, A. B., 1982. Dehydration melting of pelitic rocks and the generation of H_2O-undersaturated granitic liquids. *American Journal of Science*, **282,** 1567–1595.
Todt, W., 1976. Zirkon-U/Pb-Alter des Malsburg-Granits vom Südschwarzwald. *Neues Jahrbuch für Mineralogie, Monatshefte*, **12,** 532–544.
Todt, W. & Büsch, W., 1981. U–Pb investigations on zircons from pre-Variscan gneisses—A study from the Schwarzwald, West Germany. *Geochimica et Cosmochimica Acta*, **45,** 1789–1801.
Tsuchiyama, A. & Takahashi, E., 1983. Melting kinetics of a plagioclase feldspar. *Contributions to Mineralogy and Petrology*, **84,** 345–354.
Tuttle, O. F. & Bowen, L. N., 1958. Origin of granite in the light of experimental studies in the system $NaAlSi_3O_8$–$KAlSi_3O_8$–SiO_2-H_2O. Geological Society of America, *Memoir*, **74**.
Vernon, R. H. & Collins, W. J., 1988. Igneous microstructures in migmatites. *Geology*, **16,** 1126–1129.
Von Drach, V., 1978. Mineral-Alter im Schwarzwald. *Unpubl. PhD Thesis, University of Heidelberg*.
Wendt, I., Lenz, H. & Höhndorf, A., 1974. Das Alter des Bärhalde-Granites, (Schwarzwald) und der Uranlagerstätte Menzenschwand. *Geologisches Jahrbuch*, **E2,** 131–143.
Wickert, F. & Eisbacher, G. H., 1988. Two-sided Variscan thrust tectonics in the Vosges Mountains, northeastern France. *Geodinamica Acta*, **2,** 101–120.
Wimmenauer, W. & Stenger, R., 1989. Acid and intermediate HP metamorphic rocks in the Schwarzwald, Federal Republic of Germany). *Tectonophysics*, **157,** 109–116.
York, D., 1969. Least squares fitting of a straight line with correlated errors. *Earth and Planetary Science Letters*, **5,** 320–324.
Yund, R. A. & Tullis, J., 1991. Compositional changes of minerals associated with dynamic recrystallization. *Contributions to Mineralogy and Petrology*, **108,** 346–355.

Received 30 November 1993; revision accepted 17 March 1994.

APPENDIX

Analytical techniques for microprobe work

Mineral analyses were performed using a Camebax SX 50 microprobe equipped with four spectrometers. Operating parameters were: 20 s counting time (15 s for Na, K), 10 nA beam current and 15 kV accelerating voltage. PAP correction was applied to the data. Analyses were calibrated against natural and synthetic oxide and silicate standards. Feldspar compositions were calculated on the basis of 8 oxygens assuming all Fe to be Fe^{3+}. Biotite compositions were calculated on the basis of 11 oxygens assuming a fixed ratio of $Fe^{3+}/Fe_{tot} = 0.15$.

Analytical techniques for isotope studies

Monazite separates were prepared from 5 kg of sample material by crushing and sieving as well as by conventional magnetic and heavy-liquid separation techniques. Separates were hand picked, leached in an H_2O/HNO_3 mixture, cleaned ultrasonically in ultrapure acetone, and digested by HCl in teflon vessels in steel autoclaves at 180° C. A $^{235}U/^{208}Pb$ spike solution was added before dilution to determine element concentrations. Chemical separation of U and Pb by cation exchange techniques followed largely the procedure described by Krogh (1973). Pb isotope ratios were corrected for 0.012% fractionation per mass unit as deduced from measured standard values of NBS 981 ($^{204}Pb/^{206}Pb = 0.05188 \pm 28$, $^{207}Pb/^{206}Pb = 0.91372 \pm 10$, $^{208}Pb/^{206}Pb = 2.16252 \pm 44$). Total procedural blanks were <40 pg for Pb and 15 pg for U. A Pb blank correction was applied to the data (isotopic composition of blank Pb: $^{208}Pb/^{204}Pb = 37.5$, $^{207}Pb/^{204}Pb = 15.52$, $^{206}Pb/^{204}Pb = 17.72$). The model of Stacey & Kramers (1975) was used for common lead correction. Errors as quoted in Table 3 were calculated using the procedure of Ludwig (1980). All ages were calculated using the decay constants given by Steiger & Jäger (1977).

For Rb–Sr analyses, thin-slabs corresponding to leucosomes and mesosomes, respectively, were cut from profiles of two migmatite samples (see Table 2). Half of each profile was left for petrographic and microprobe work. The thin-slabs were separately crushed and powdered. After adding a $^{87}Rb/^{84}Sr$-spike solution for determination of element concentrations, a HF/HNO_3 mixture was used for digestion in Savillex screw-top teflon containers. Rb and Sr were chemically separated by conventional cation exchange techniques using quartz glass columns, cation exchange resin and HCl. A linear correction for mass fractionation was applied to $^{87}Sr/^{86}Sr$ ratios by normalizing to a $^{86}Sr/^{88}Sr$ value of 0.1194. Measured $^{87}Sr/^{86}Sr$ ratios for NBS standard 987 were 0.710269 ± 23 (Teledyne machine) and 0.710276 ± 9 (VG machine). Rb ratios were corrected for 0.6% fractionation per mass unit as deduced from measured values of Rb standard NBS 984 of 2.6086 ± 80. Total procedural blanks were less than 200 pg for Sr ($^{87}Sr/^{86}Sr$ ratio of blank: 0.710) and 20 pg for Rb. Errors for $^{87}Rb/^{86}Sr$ ratios are estimated at maximum 1% on the basis of reproducibility of sample ratios. Quoted errors for $^{87}Sr/^{86}Sr$ ratios comprise 2σ analytical errors, uncertainties in the isotopic composition of Sr in the spike solution as well as a blank correction. Isochrons were calculated using the method of York (1969). All decay constants used are those reported by Steiger & Jäger (1977). For Sr profile diagrams (see Figs 5 & 6) the measured $^{87}Sr/^{86}Sr$ ratios of the individual slabs were calculated for different stages in the past using the respective $^{87}Rb/^{86}Sr$ values. Error enlargement calculations for these back-calculated $^{87}Sr/^{86}Sr$ ratios include errors of the measured $^{87}Sr/^{86}Sr$ ratios as well as errors for the $^{87}Rb/^{86}Sr$ ratios.